





TECHNICAL NOTE

Caveat emptor!—wobble-matching European wood samples (AD 46–AD 286)

Alex Bayliss¹, David Brown², Michael Dee³, Peter Marshall¹ and Lukas Wacker⁴

¹Historic England, Cannon Bridge House, 25 Dowgate Hill, London, EC4R 2YA, UK, ²School of Natural and Built Environment, The Queen's University, Belfast, BT7 1NN, UK, ³Centre for Isotope Research, University of Groningen, Nijenborgh 6, 9747 AG Groningen, Netherlands and ⁴Laboratory of Ion Beam Physics, ETH Zürich, Otto-Stern-Weg 5, 8093 Zürich, Switzerland

Corresponding author: Alex Bayliss; Email: Alex.Bayliss@HistoricEngland.org.uk

Received: 26 November 2023; **Revised:** 19 March 2024; **Accepted:** 22 March 2024; **First published online:** 08 October 2024

Keywords: accuracy; calibration; dendrochronology

Abstract

This study suggests that there may be considerable difficulties in providing accurate calendar age estimates in the Roman period in Europe, between ca. AD 60 and ca. AD 230, using the radiocarbon calibration datasets that are currently available. Incorporating the potential for systematic offsets between the measured data and the calibration curve using the ΔR approach suggested by Hogg et al. (2019), only marginally mitigates the biases in calendar date estimates observed. At present, it clearly behoves researchers in this period to “*caveat emptor*” and validate the accuracy of their calibrated radiocarbon dates and chronological models against other sources of dating information.

Introduction

The current radiocarbon calibration curve for the Northern Hemisphere, IntCal20 (Reimer et al. 2020), represents a major update of previous calibration curves (Reimer et al. 2004; Reimer et al. 2013). Over the first half of the first millennium AD, IntCal20 is based on over 550 calibration datapoints, in comparison to IntCal13, which was based on just over 100 (Figure 1 [upper]). The data included in IntCal13 were measured on decadal and bi-decadal blocks of wood, whereas IntCal20 also includes measurements on 5-year blocks for the entire half millennium, and measurements on single-year tree-rings between AD 290 and AD 486. A new statistical approach for the construction of the curve has also been adopted (Heaton et al. 2020).

In general, the calibration data and, thus, the two curves follow each other closely. There is, however, a more appreciable divergence between ca. AD 60 and ca. AD 230. As previously observed (Haneca et al. 2021; Staff and Liu 2021), this can lead to archaeologically meaningful differences in calibrated radiocarbon dates in this period. Modeling can exacerbate this issue, as demonstrated recently for a small cemetery (Group A) at Stanwick, Northamptonshire, which falls in the decades around AD 130 if modeled using IntCal13 or in the decades around AD 200 if modeled using IntCal20 (Fleming et al. submitted, fig. 5; Figure 2). The results from the two models are clearly incompatible, and both cannot be correct.

The Dataset

In order to compare the effectiveness of IntCal13 and IntCal20 for producing accurate calibration in the Roman period in Europe, a series of wobble-match models were constructed using ¹⁴C measurements on known-age tree-rings from the Irish oak chronology (Baillie 1982; Brown and Baillie 2012; Pilcher et al. 1984).

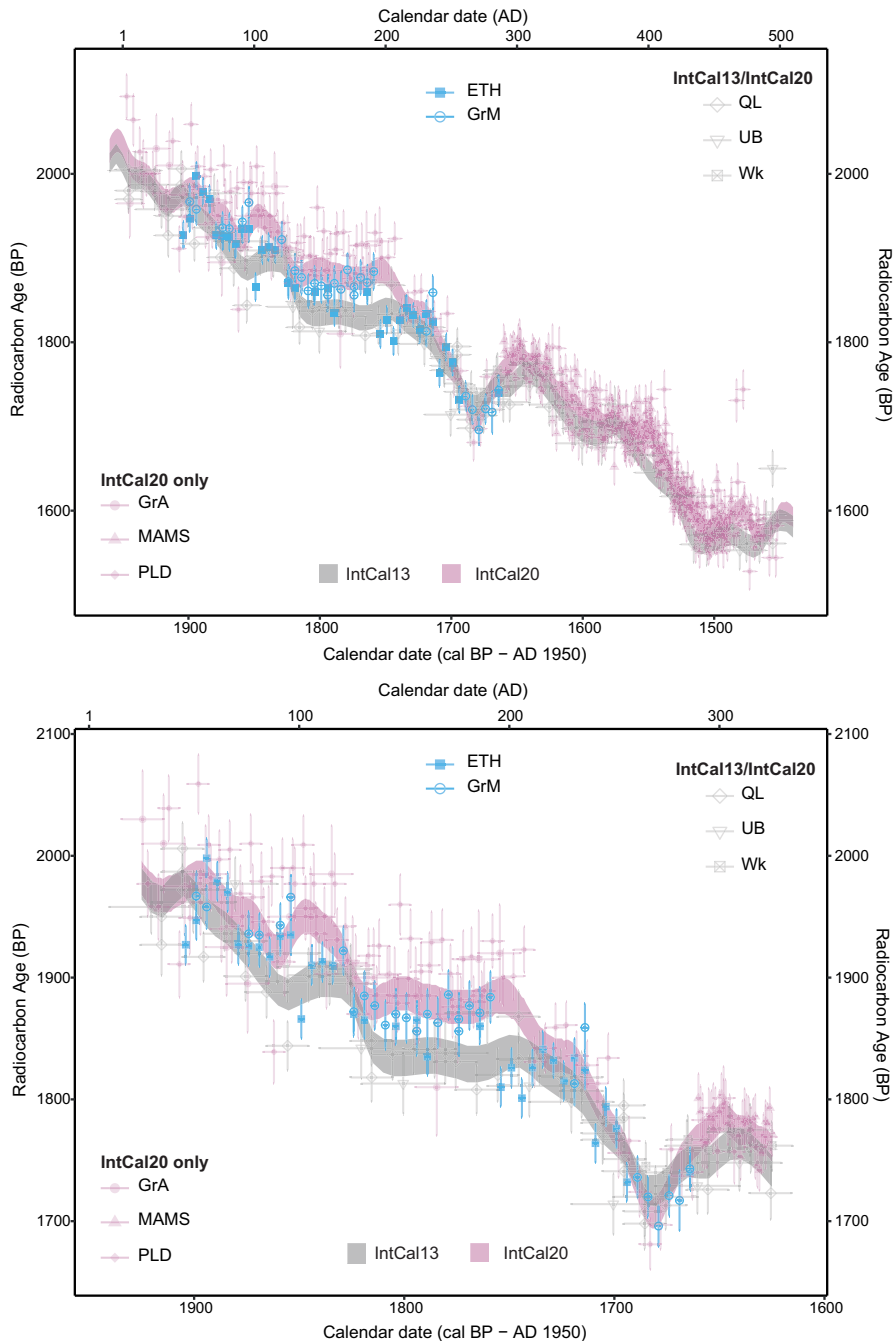


Figure 1. *IntCal20* (magenta-pink) and *IntCal13* (grey) with the calibration datasets on which they are based; those from Seattle (QL; Stuiver and Braziunas 1993; Stuiver et al. 1998), Belfast (UB; McCormac et al. 2004; Pearson et al. 1986) and Waikato (Wk; Hogg et al. 2009) are included in both curves, those from Groningen (GrA; Sakamoto et al. 2003), Mannheim (MAMS-; Friedrich et al. 2019) and Palaeo Labo Co. Ltd (Sakamoto et al. 2003; Okuno et al. 2018) only in *IntCal20*. Measurements on Irish oak undertaken for this study are shown in blue (ETH- and GrM-). The first half of the first millennium AD (upper), the period of this study (lower).

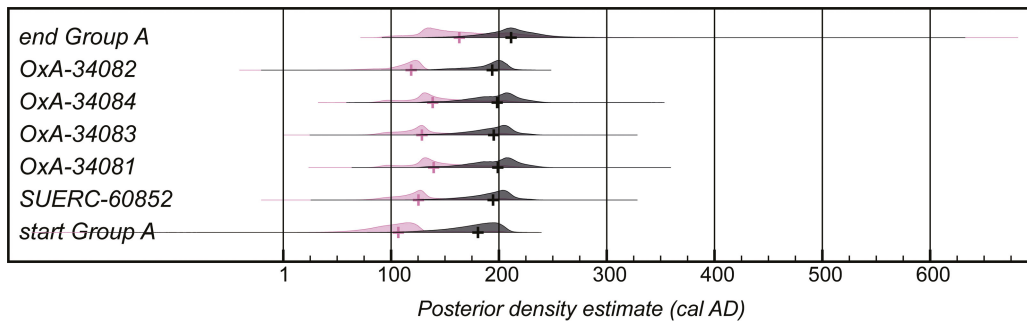


Figure 2. Probability distributions of dates from burials in Group A at Stanwick, Northamptonshire, UK, derived from the model defined in Fleming et al. (submitted, fig 5). Each distribution represents the relative probability that an event occurs at a particular time. Distributions in magenta-pink derive from the model calculated using IntCal13 (Reimer et al. 2013), and those in black from the model calculated using IntCal20 (Reimer et al. 2020). Crosses indicate the medians of the posterior distributions.

The samples were of latewood from single tree-rings that have been dated by dendrochronology as forming between AD 46 and AD 286. Every fifth ring was dated, except in two cases where the gap was seven and three rings respectively (Appendix 1). The samples came from four bog oaks (Q815, Q821, Q837, and Q1081) recovered from a demolished cottage at Balloo, Co Down (52.47°N, 5.71°W), four bog oaks (Q9881, Q9985–6, and Q9888) from the lake edge at Ballinderry, Co Antrim (54.55°N, 6.28°W), and a single waterlogged oak (Q451) from those recovered from Allistragh, Co Armagh (54.23°N, 6.40°W). Details of the dendrochronological dating and sub-sampling for radiocarbon dating of the timbers from Balloo and Ballinderry can be found in Supplementary Material; details for the timber from Allistragh are published elsewhere (Wacker et al. 2020, Supplementary Material).

Radiocarbon dating of the samples of Irish oak was undertaken by the Centre for Isotope Research, University of Groningen (GrM-), the Netherlands, and at the Laboratory of Ion Beam Physics, ETH Zürich (ETH-), Switzerland in 2022. In Groningen, each ring was converted to α -cellulose using an intensified acid-base-acid-oxidation pretreatment (Dee et al. 2020) and combusted in an elemental analyser (IsotopeCube NCS), coupled to an Isotope Ratio Mass Spectrometer (Isoprime 100). The resultant CO_2 was graphitised by hydrogen reduction in the presence of an iron catalyst (Hut et al. 1986; Aerts-Bijma et al. 1997). The graphite was then pressed into aluminium cathodes and dated by Accelerator Mass Spectrometry (AMS) (Synal et al. 2007; Salehpour et al. 2016). In Zürich, cellulose was extracted from each ring using the base-acid-base-acid-bleaching (BABAB) method described by Němec et al. (2010), combusted and graphitised as outlined in Wacker et al. (2010c) and dated by accelerator mass spectrometry (Synal et al. 2007; Wacker et al. 2010a). At both laboratories data reduction was undertaken as described by Wacker et al. (2010b), and both facilities maintain continual programmes of quality assurance procedures (Aerts-Bijma et al. 2021, Sookdeo et al. 2020), in addition to participation in international inter-comparison exercises (Wacker et al. 2020).

The results are conventional ^{14}C ages, corrected for fractionation using $\delta^{13}\text{C}$ values measured by accelerator mass spectrometry (Stuiver and Polach 1977; Appendix 1). Fifteen tree-rings were measured by both laboratories, all pairs being consistent at the 5% significance level (Ward and Wilson 1978). The weighted mean difference between these replicates is -7.97 ± 6.36 BP (ETH younger), and χ^2_{red} is 0.75 (Bevington and Robertson 1992, equation 4.19; Bevington 1969, 69).

Wiggle-Matching

Wiggle-matching has been undertaken using the Bayesian approach first described by Christen and Litton (1995), implemented using OxCal v4.4 (Bronk Ramsey et al. 2001; Bronk Ramsey 2009).

This method assumes that we have independent pointwise estimates of the calibration curve: covariance information from the calibration curve is not used (Millard 2008; Muzikar and Heaton 2022).

The models all contain measurements on seven tree-rings, spaced five years apart and spanning 31 calendar years (except those between AD 166–198 and AD 176–206 and those between AD 198–226 and AD 208–236 which span 33 calendar years and 29 calendar years respectively and contain some measurements spaced three years apart and seven years apart). This short span of calendar dating has been chosen to replicate archaeological reality, for example when wiggle-matching tree-ring sequences that are usually undatable by ring-width or oxygen isotope dendrochronology (Bayliss et al. 2017), or when wiggle-matching different elements of a human skeleton (Millard et al. 2020). All models calculate the date when the ring for AD 286 formed. Replicate measurements have been combined by taking a weighted mean before inclusion in the model. The 43 wiggle-matches run from AD 46–AD 76, AD 51–AD 81 etc. to AD 256–AD 286. Each model has been calculated three times: once using IntCal13, once using IntCal20, and once using IntCal20 allowing for a potential systematic offset between the new data and the calibration curve (applying the “Delta_R” function of OxCal with a uniform prior of -20 to $+20$ BP; Hogg et al. 2019). All models have been run at a resolution of 1 and for 20M iterations.

Figure 3 shows the wiggle-match model that includes measurements on samples dating to between AD 76 and AD 106, and so there are 180 rings until the formation of the ring for AD 286. In this case, the model calculated using IntCal13 (lower), the model calculated using IntCal20 (middle), and the model calculated using IntCal20 allowing for a potential systematic offset (upper), all clearly provide dating that is incompatible with the dendrochronological age for the formation of the ring for AD 286. The date estimate provided using IntCal13 is too early, and those provided using IntCal20 are too late.

The highest posterior density intervals for the ring for AD 286 from all 43 models, calculated using the three calibration approaches are provided in Appendix 2. The true value lies outside these intervals more often than expected (Table 1). The posterior distributions for the ring for AD 286 are illustrated in Figure 4. Those where the true date lies outside the Highest Posterior Density intervals at 95% probability are shown in magenta-pink. Again, it is clear that the wiggle-match results produced using IntCal13 are biased towards older ages, and that those produced using IntCal20 are biased towards younger ages. The use of the ΔR approach to allow for a potential systematic offset between the new data and the calibration curve marginally mitigates, but does not resolve, the younger bias in the dating produced using IntCal20.

Discussion

The greater quantity of data in IntCal20 means that it is usually more robust than IntCal13, although this case study demonstrates that producing accurate dating in the period between ca. AD 60 and ca. AD 230 is challenging using either calibration curve. Replication shows that the new data produced in Groningen and Zürich are consistent within the quoted uncertainties, which are of a similar scale to those reported for the calibration datasets (averages GrM: ± 19 BP, ETH: ± 19 BP; Table 2).

The reason that IntCal20 diverges from IntCal13 in this period is that it includes additional data from two Japanese trees (HKN-1, Japanese cedar, and NNMSM-TR1, Japanese cypress), which produce older ages than the data we have from North American trees (RC and SR, Giant Redwood) and European trees (Q451, Q455, Q218, and Q9887, oak), which were included in both IntCal13 and IntCal20, only during the late first and second centuries AD. The datasets are more compatible at later times, including with the single-year data on European trees measured in Mannheim (MAMS-; Figure 1 [upper]).

Systematic offsets can arise from laboratory biases, but also from geographic offsets. In this case, significant systematic laboratory bias is perhaps less likely since the data have been measured in more than one laboratory, and the data from the same trees measured in those same laboratories are in good agreement in the third and fourth centuries AD (Figure 1 [upper]). The Global Circulation Model of

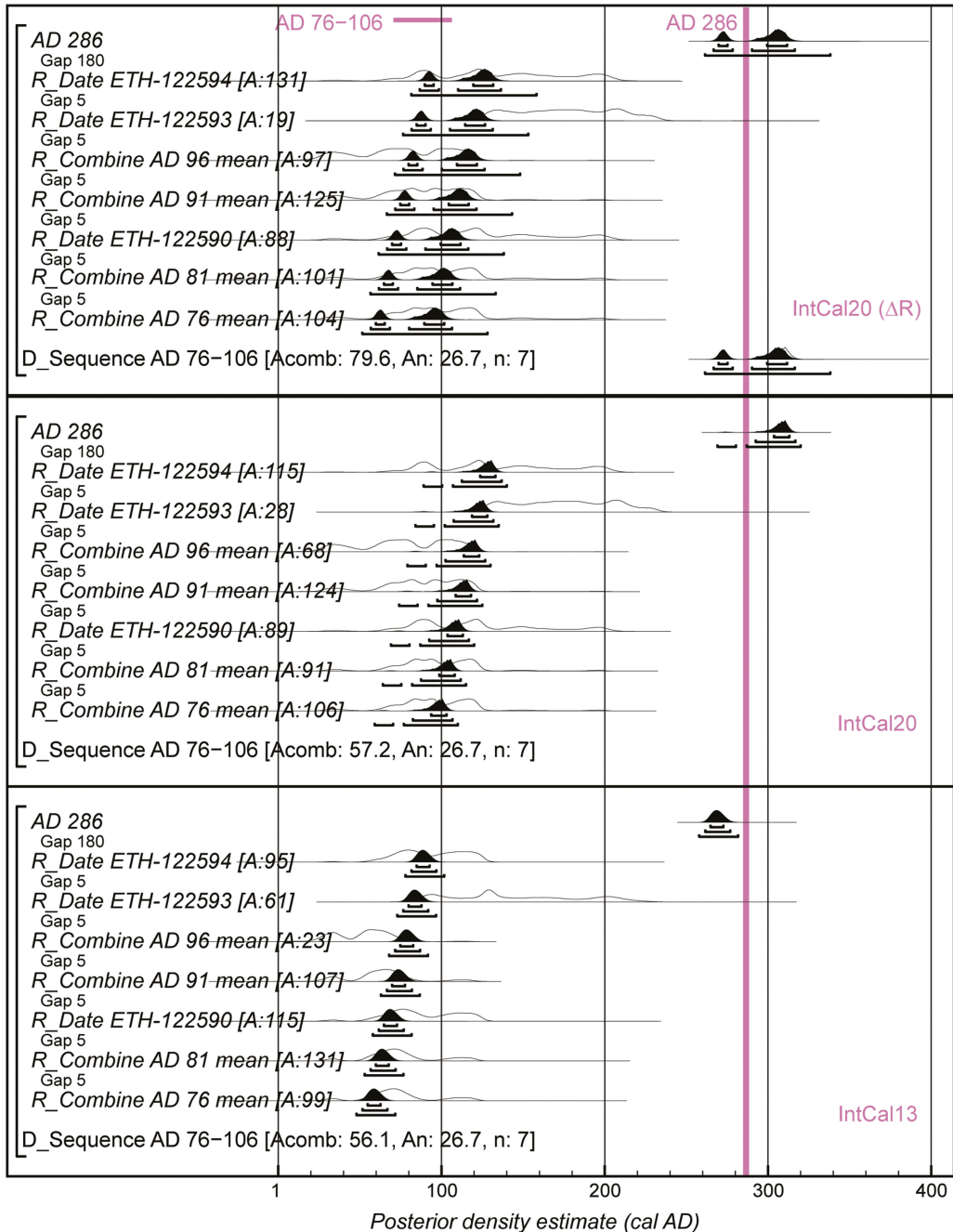


Figure 3. Probability distributions of dates from AD 76–106. Each distribution represents the relative probability that an event occurs at a particular time. For each of the dates two distributions have been plotted: one in outline, which is the result of simple radiocarbon calibration, and a solid one, based on the wiggle-match sequence. Distributions other than those relating to particular samples, correspond to aspects of the model. For example, the distribution “AD 286” is the estimated date when the ring for AD 286 formed. The model has been calculated using IntCal13 (lower), IntCal20 (middle), and IntCal20 with an allowance for a potential systematic offset (upper).

Table 1. Number of models where the known-age of AD 286 is not included in the Highest Posterior Density intervals (rounded outwards to the nearest year)

	Highest Posterior Density intervals		
	68%	95%	99%
IntCal13	30	16	6
IntCal20	27	18	10
InCal20 (ΔR)	21	13	5
Expected	13–14	1–2	<1

Braziunas et al. (1995) predicted a decline in atmospheric ^{14}C of ca. 8 BP per 10° of latitude, but such a meridional trend has proved difficult to demonstrate in practice (but see Büntgen et al. 2018, fig 3; Pearson et al. 2020, table 1). In this case a simple latitudinal trend seems unlikely, because IntCal13 in this period is dominated by measurements on Giant Redwoods (from 36°N) and IntCal20 is dominated by measurements on Japanese trees (from 35°N). These datasets differ as much from each other as they do from the data on the Irish oak (from 52°N – 54°N) (Figure 1 [lower]).

The offsets between the datasets included in IntCal20 anyway appear to vary through time. This is also apparent in the new dataset on Irish oak (Figure 5), which is significantly older than IntCal13 in the late first and second century AD, and significantly younger than IntCal20 in the second and earlier third century AD. Nakamura et al. (2013) have previously suggested that there may be a time-variable offset in Japanese trees, perhaps arising from variations in the East Asian monsoon, and Miyake et al. (2014, 1192) similarly observe that data on Japanese trees were older than IntCal13, but this would not explain the differences observed between IntCal13 and our new dataset.

It is also possible that there is annual variation in ^{14}C which is currently not captured by the calibration curves as they are not visible in the blocked data that are currently available (Table 2). This may be the reason why some of the models calculated using IntCal20 and allowing for a systematic offset between the new dataset and the calibration curve have poor overall agreement (Table 2). If so, this may suggest that more year-to-year variation in atmospheric ^{14}C content may be expected in the decades around AD 100. Generally, detailed understanding of the short-term variations in the shape of the calibration curve is critical for providing precise and accurate chronologies in situations where an archaeological site, or the available archaeological sequence, spans only a few decades.

Conclusions

This study suggests that there may be considerable difficulties in providing accurate calendar age estimates in the period between ca. AD 60 and ca. AD 230 using the radiocarbon calibration datasets that are currently available. It is possible that there may be locational differences in atmospheric radiocarbon that are important for archaeological interpretation at this time, although further work is clearly required to understand the observed variation. Incorporating the potential for systematic offsets between the measured data and the calibration curve using the ΔR approach suggested by Hogg et al. (2019), only marginally mitigates the biases in calendar date estimates observed (and it should be noted that this approach was not actually adopted in the statistical methodology used for constructing IntCal20 [Heaton et al. 2020]).

At present, it clearly behoves researchers in this period to “*caveat emptor*” and validate the accuracy of their calibrated radiocarbon dates and chronological models against other sources of dating information, such as the *termini post quos* provided by coins issued by known historical figures and documentary evidence where this is available.

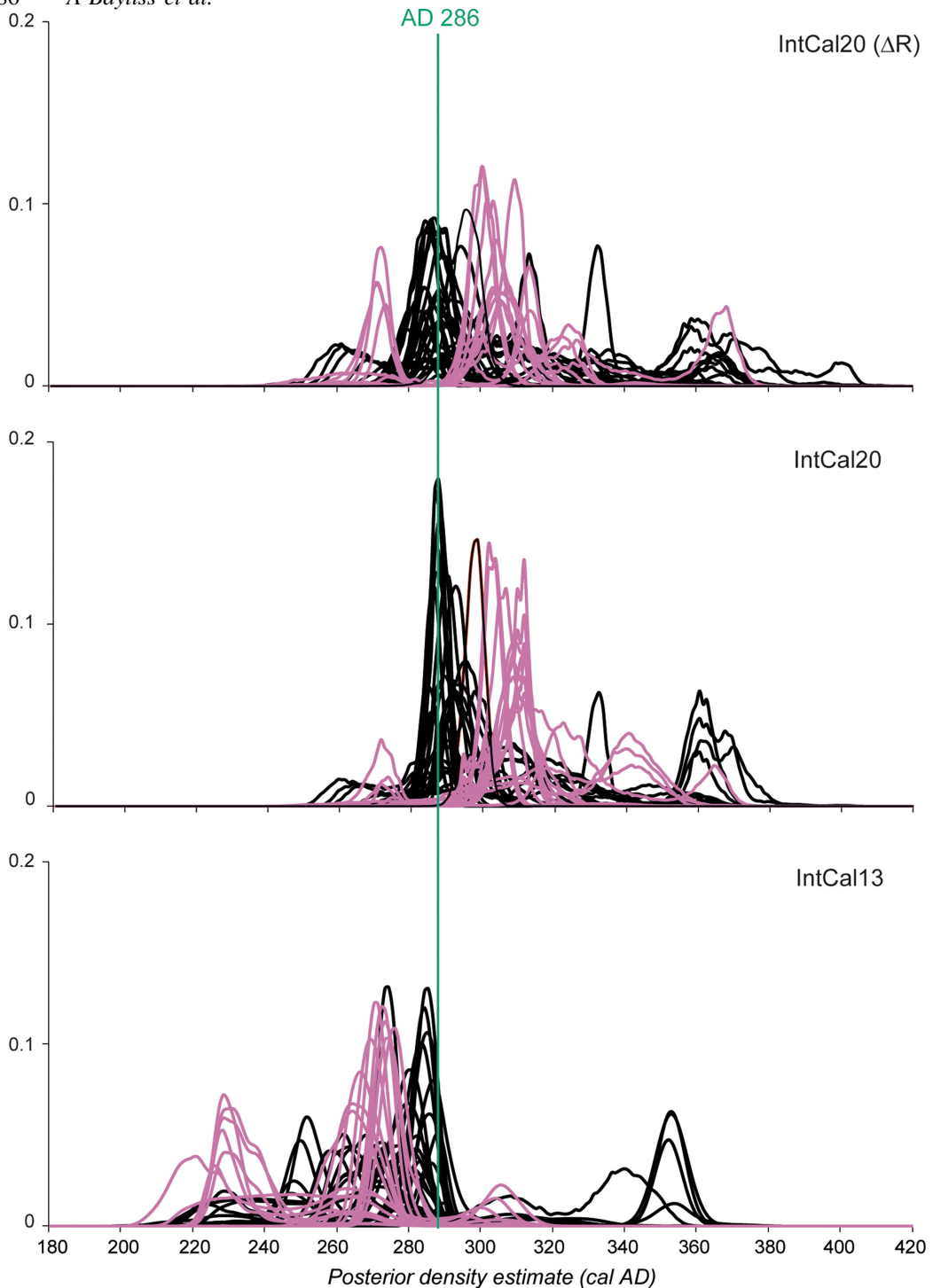


Figure 4. Posterior density estimates for the ring formed in AD 286, from wiggle-matching measurements from seven rings spanning successive 31-year blocks between AD 46–76 and AD 256–286 ($A_{\text{comb}} > A_n$: 26.7, n : 7 for all), calculated using *IntCal13* (lower), *IntCal20* (middle), and *IntCal20* with an allowance for a potential systematic offset (upper). Five of the models calculated using *IntCal20* allowing a potential systematic offset (ΔR) have poor overall agreement (see Appendix 2). Distribution where the true date lies within the Highest Posterior Density intervals at 95% probability are shown in black, those where it is outside these intervals in magenta-pink.

Table 2. Summary of calibration data included in *IntCal13* and *IntCal20* AD 46–286 (* average uncertainty includes reported error multiplier)

Dataset	Laboratory	Method	Tree (species)	Lat./Long.	Resolution	N	Average uncertainty	References
1-8	QL-	GPC	RC (<i>Sequoiadendron giganteum</i>)	36.7°N, 118.9°W	Decadal	6	19*	Stuiver and Braziunas 1993
1-9	QL-	GPC	SR (<i>Sequoiadendron giganteum</i>)	36.5°N, 118.5°W	Decadal	23		Stuiver et al. 1998 Stuiver and Braziunas 1993
2-3	UB-	LSS	Q451 (<i>Quercus</i> sp.)	54.2°N, 6.4°W	Bi-decadal	4	24*	Pearson et al. 1986
			Q455 (<i>Quercus</i> sp.)	54.2°N, 6.4°W		6		
			Q218 (<i>Quercus</i> sp.)	54.3°N, 7.6°W		3		
3-2	Wk-	LSS	Q9887 (<i>Quercus</i> sp.)	54.6°N, 6.3°W	Decadal	5	20	Hogg et al. 2009
65-2	PLD-	AMS	HKN-1 (<i>Cryptomeria japonica</i>)	35.8°N, 137.9°E	5-year	29	24	Okuno et al. 2018
65-4	PLD-	AMS	NNMSM-TR1 (<i>Chamaecyparis obtuse</i>)	35.3°N, 137.9°E	5-year	48		Okuno et al. 2018
65-3	GrA-	AMS	HKN-1 (<i>Cryptomeria japonica</i>)	35.8°N, 137.9°E	Decadal	16	40	Sakamoto et al. 2003

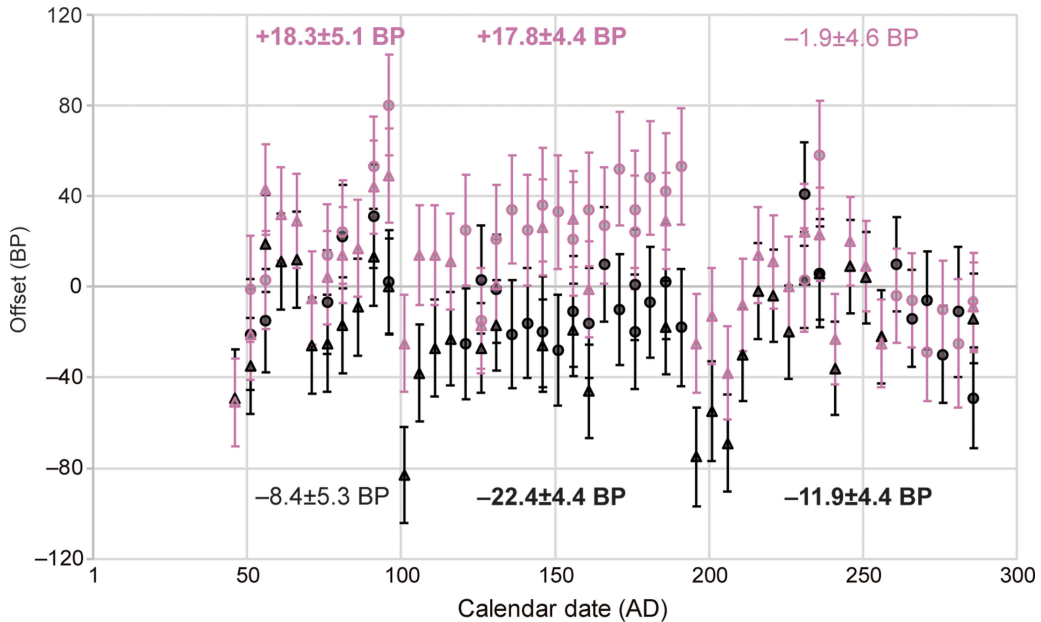


Figure 5. Offsets between the data presented in Appendix 1 and IntCal13 (magenta-pink) and IntCal20 (black) (ETH = triangles, GrM = circles). Weighted mean offsets shown in bold are statistically significant at the 5% significance level.

Supplementary material. To view supplementary material for this article please visit <https://doi.org/10.1017/RDC.2024.54>.

Acknowledgments. We are grateful to Historic England for funding this research (402951-2017), and to members of the radiocarbon groups at ETH Zürich and the University of Groningen for processing and dating the samples.

References

- Aerts-Bijma AT, Meijer HAJ and van der Plicht J (1997) AMS sample handling in Groningen. *Nuclear Instruments and Methods in Physics Research B* **123**:221–225. [https://doi.org/10.1016/S0168-583X\(96\)00672-6](https://doi.org/10.1016/S0168-583X(96)00672-6).
- Aerts-Bijma AT, Paul D, Dee MW, Palstra SWL and Meijer HAJ (2021) An independent assessment of uncertainty for radiocarbon analysis with the new generation high-yield accelerator mass spectrometers. *Radiocarbon* **63**(1), 1–22. <https://doi.org/10.1017/RDC.2020.101>.
- Baillie MGL (1982) *Tree-Ring Dating and Archaeology*. London: Croom Helm.
- Bayliss A, Marshall P, Tyers C, Bronk Ramsey C, Cook G, Freeman SPHT and Griffiths S (2017) Informing conservation: towards ^{14}C wiggle-matching of short tree-ring sequences from medieval buildings in England. *Radiocarbon* **59**(3), 985–1007. <https://doi.org/10.1017/RDC.2016.61>.
- Bevington PR (1969) Propagation of errors. In Bevington PR (ed), *Data Reduction and Error Analysis for the Physical Sciences*. New York: McGraw-Hill, 56–65.
- Bevington PR and Robinson DK (1992) *Data Reduction and Error Analysis for the Physical Sciences*. Boston: WCB/McGraw-Hill.
- Braziunas TF, Fung IY and Stuiver M (1995) The preindustrial atmospheric $^{14}\text{CO}_2$ latitudinal gradient as related to exchanges among atmospheric, oceanic, and terrestrial reservoirs. *Global Biogeochemical Cycles* **9**(4), 565–584. <https://doi.org/10.1029/95GB01725>.
- Bronk Ramsey C (2009) Bayesian analysis of radiocarbon dates. *Radiocarbon* **51**(1), 337–360. <https://doi.org/10.1017/S0033822200033865>.
- Bronk Ramsey C, van der Plicht J and Weninger B (2001) “Wiggle matching” radiocarbon dates. *Radiocarbon* **43**(2), 381–391. <https://doi.org/10.1017/S0033822200038248>.
- Brown DM and Baillie MGL (2012) Confirming the existence of gaps and depletions in the Irish oak tree-ring record. *Dendrochronologia* **30**(2), 85–91. <https://doi.org/10.1016/j.dendro.2010.09.003>.
- Büntgen U, Wacker L, Galván JD, Arnold S, Arseneault D, Baillie M, Beer J, Bernabei M, Bleicher N and Boswijk G et al (2018) Tree rings reveal globally coherent signature of cosmogenic radiocarbon events in 774 and 993 CE. *Nature Communications* **9**(1), 3605. <https://doi.org/10.1038/s41467-018-06036-0>.

- Christen JA and Litton CD (1995) A Bayesian approach to wiggle-matching. *Journal of Archaeological Science* **22**(6), 719–725. [https://doi.org/10.1016/0305-4403\(95\)90002-0](https://doi.org/10.1016/0305-4403(95)90002-0)
- Dee MW, Palstra SWL, Aerts-Bijma AT, Bleeker MO, de Bruijn S, Ghebru F, Jansen HG, Kuitens M, Paul D and Richie RR et al (2020) Radiocarbon dating at Groningen: New and updated chemical pretreatment procedures. *Radiocarbon* **62**(1), 63–74. <https://doi.org/10.1017/RDC.2019.101>
- Fleming R, Crosby V, Bayliss A, Mays S, Bronk Ramey C, Dunbar E, Cool HEM and Wardle A (submitted) Establishing a chronology for roman and post-Roman Stanwick, Northamptonshire. Britannia.
- Friedrich R, Kromer B, Sirocko F, Esper J, Lindauer S, Nievergelt D, Heussner KU and Westphal T (2019) Annual ^{14}C tree-ring data around 400 AD: Mid- and high-latitude records. *Radiocarbon* **61**(5), 1305–1316. <https://doi.org/10.1017/RDC.2019.34>
- Haneca K, Ervynck A, Boudin M, de Winter N, Martens M and Vanderhoeven A (2021) The impact of the new Intcal20 calibration curve upon the interpretation of radiocarbon dates from the roman period. *Signa* **10**, 101–121.
- Heaton TJ, Blaauw M, Blackwell PG, Bronk Ramsey C, Reimer PJ and Scott EM (2020) The intcal20 approach to radiocarbon calibration curve construction: A new methodology using Bayesian splines and errors-in-variables. *Radiocarbon* **62**(4), 821–863. <https://doi.org/10.1017/RDC.2020.46>.
- Hogg A, Palmer J, Boswijk G, Reimer P and Brown D (2009) Investigating the interhemispheric ^{14}C offset in the 1st millennium AD and assessment of laboratory bias and calibration errors. *Radiocarbon* **51**(4), 1177–1186. <https://doi.org/10.1017/S0033822200034238>.
- Hogg AG, Heaton TJ, Ramsey CB, Boswijk G, Palmer JG, Turney CSM, Southon J and Gumbley W (2019) The influence of calibration curve construction and composition on the accuracy and precision of radiocarbon wiggle-matching of tree rings, illustrated by Southern Hemisphere atmospheric data sets from AD 1500–1950. *Radiocarbon* **61**(5), 1265–1291. <https://doi.org/10.1017/RDC.2019.42>.
- Hut G, Göte Östland H and van der Borgh K (1986) Fast and complete CO_2 -to-graphite conversion for ^{14}C accelerator mass spectrometry. *Radiocarbon* **28**(2A), 186–190. <https://doi.org/10.1017/S0033822200007256>.
- McCormac FG, Bayliss A, Baillie MGL and Brown DM (2004) Radiocarbon calibration in the Anglo-Saxon period: AD 495–725. *Radiocarbon* **46**(3), 1123–1125. <https://doi.org/10.1017/S0033822200033051>.
- Millard AR, Annis RG, Caffell AC, Dodd LL, Fischer R, Gerrard CM, Graves CP, Hendy J, Mackenzie L, Montgomery J, Nowell GM, Radini A, Beaumont J, Koon HEC and Speller CF (2020) Scottish Soldiers from the Battle of Dunbar 1650: a prosopographical approach to a skeletal assemblage. *PlosOne*. <https://doi.org/10.1371/journal.pone.0243369>.
- Millard AR (2008) Comment on article by Blackwell and Buck. *Bayesian Analysis* **3**(2), 255–262. <https://doi.org/10.1214/08-BA309B>.
- Miyake F, Masuda K, Hakozaiki M, Nakamura T, Tokanai F, Kato K, Kimura K, Mitsutani T (2014) Verification of the Cosmic-Ray Event in AD 993–994 by Using a Japanese Hinoki Tree. *Radiocarbon* **56**(3), 1189–1194. <https://doi.org/10.2458/56.17769>.
- Muzikar P and Heaton TJ (2022) Wiggle matching with correlations. *Radiocarbon* **64**(1), 187–194. <https://doi.org/10.1017/RDC.2021.106>.
- Nakamura T, Masuda K, Miyake F, Nagaya K and Yoshimitsu T (2013) Radiocarbon ages of annual rings from Japanese wood: Evident age offset based on intcal09. *Radiocarbon* **55**(2), 763–770. <https://doi.org/10.1017/S0033822200057921>.
- Němec M, Wacker L, Hajdas I and Gäggeler H (2010) Alternative methods for cellulose preparation for ams measurement. *Radiocarbon* **52**, 1358–1370. <https://doi.org/10.1017/S0033822200046440>.
- Okuno M, Hakozaiki M, Miyake F, Kimura K, Masuda K, Sakamoto M, Hong W, Yatsuzuka S and Nakamura T (2018) Chronological significance of ^{14}C spike and precise age determination of the b-tm tephra, China/North Korea. Abstracts of the 23rd International Radiocarbon Conference. Trondheim, 52.
- Pearson C, Wacker L, Bayliss A, Brown D, Salzer M, Brewer P, Bollhalder S, Boswijk G and Hodgins G (2020) Annual variation in atmospheric ^{14}C between 1700 BC and 1480 BC. *Radiocarbon* **62**(4), 939–952. <https://doi.org/10.1017/RDC.2020.14>.
- Pearson GW, Pilcher JR, Baillie MGL, Corbett DM and Qua F (1986) High-precision ^{14}C measurements of Irish oaks to show the natural ^{14}C variations from AD 1840 to 5210 BC. *Radiocarbon* **28**, 911–934. <https://doi.org/10.1017/S0033822200060197>.
- Pilcher JR, Baillie MGL, Schmidt B and Becker B (1984) A 7,272-year tree-ring chronology for western Europe. *Nature* **312**(5990), 150–152. <https://doi.org/10.1038/312150a0>.
- Reimer P, Baillie MGL, Bard E, Bayliss A, Beck JW, Bertrand CJH, Blackwell PG, Buck CE, Burr GS and Cutler KB et al (2004) Radiocarbon calibration from 0–26 cal kyr BP—IntCal04 terrestrial radiocarbon age calibration, 0–26 cal kyr BP. *Radiocarbon* **46**(3), 1029–1059. <https://doi.org/10.1017/S0033822200032999>.
- Reimer PJ, Austin WEN, Bard E, Bayliss A, Blackwell PG, Bronk Ramsey C, Butzin M, Cheng H, Edwards RL and Friedrich M et al (2020) The Intcal20 northern hemisphere radiocarbon age calibration curve (0–55 cal kBP) *Radiocarbon* **64**(2), 725–757. <https://doi.org/10.1017/RDC.2020.41>.
- Reimer PJ, Bard E, Bayliss A, Beck JW, Blackwell PG, Bronk Ramsey C, Buck CE, Cheng H, Edwards RL and Friedrich M et al (2013) Intcal13 and Marine13 radiocarbon age calibration curves 0–50,000 years cal BP. *Radiocarbon* **55**(4), 1869–1887. https://doi.org/10.2458/azu_js_rc.55.16947.
- Sakamoto M, Imamura M, Van der Plicht J, Mitsutani T and Sahara M (2003) Radiocarbon calibration for Japanese wood samples. *Radiocarbon* **45**(1), 81–89. <https://doi.org/10.1017/S0033822200032410>.
- Salehpour M, Håkansson K, Possnert G, Wacker L and Synal H-A (2016) Performance report for the low energy compact Accelerator Mass Spectrometer at Uppsala University. *Nuclear Instruments and Methods in Physics Research B* **371**, 360–364. <https://doi.org/10.1016/j.nimb.2015.10.034>.

- Sookdeo A, Kromer B, Büntgen U, Friedrich M, Friedrich R, Helle G, Pauly M, Nievergelt D, Reinig F and Treydte K et al (2020) Quality dating: A well-defined protocol implemented at ETH for high-precision ^{14}C dates tested on late glacial wood. *Radiocarbon* **62**(4) 891–899. <https://doi.org/10.1017/RDC.2019.132>.
- Staff RA and Liu R (2021) Radiocarbon calibration: The next generation. *Science China Earth Sciences* **64**(3), 507–510. <https://doi.org/10.1007/s11430-020-9722-x>.
- Stuiver M and Braziunas TF (1993) Sun, ocean, climate and atmospheric $^{14}\text{CO}_2$: An evaluation of causal and spectral relationships. *The Holocene* **3**(4), 289–305. <https://doi.org/10.1177/095968369300300401>.
- Stuiver M and Polach HA (1977) Discussion reporting of ^{14}C data. *Radiocarbon* **19**(3), 355–363. <https://doi.org/10.1017/S0033822200003672>.
- Stuiver M, Reimer PJ and Braziunas TF (1998) High-precision radiocarbon age calibration for terrestrial and marine samples. *Radiocarbon* **40**(3), 1127–1151. <https://doi.org/10.1017/S0033822200019172>.
- Synal H-A, Stocker M and Suter M (2007) MICADAS: A new compact radiocarbon AMS system. *Nuclear Instruments and Methods in Physics Research B: Beam Interactions with Materials and Atoms* **259**, 7–13. <https://doi.org/10.1016/j.nimb.2007.01.138>.
- Wacker L, Bonani G, Friedrich M, Hajdas I, Kromer B, Němec M, Ruff M, Suter M, Synal HA and Vockenhuber C (2010a) MICADAS: Routine and high-precision radiocarbon dating. *Radiocarbon* **52**(2), 252–262. <https://doi.org/10.1017/S0033822200045288>.
- Wacker L, Christl M and Synal HA (2010b) Bats: A new tool for AMS data reduction. *Nuclear Instruments and Methods in Physics Research Section B: Beam Interactions with Materials and Atoms* **268**(7–8), 976–979. <https://doi.org/10.1016/j.nimb.2009.10.078>.
- Wacker L and Němec M, Bourquin J (2010c) A revolutionary graphitisation system: Fully automated, compact and simple. *Nuclear Instruments and Methods in Physics Research Section B: Beam Interactions with Materials and Atoms* **268**(7–8), 931–934. <https://doi.org/10.1016/j.nimb.2009.10.067>.
- Wacker L, Scott EM, Bayliss A, Brown D, Bard E, Bollhalder S, Friedrich M, Capano M, Cherkinsky A, Chivall D et al (2020) Findings from an in-depth annual tree ring radiocarbon intercomparison. *Radiocarbon* **62**(4), 873–882. <https://doi.org/10.1017/RDC.2020.49>.
- Ward GK and Wilson SR (1978) Procedures for comparing and combining radiocarbon age determinations: A critique. *Archaeometry* **20**(1), 19–32. <https://doi.org/10.1111/j.1475-4754.1978.tb00208>.

Appendix 1. Radiocarbon ages and stable isotopic measurements from Irish oak (AD 46–286), quoted $\delta^{13}\text{C}$ values were measured by IRMS (GrM-) or AMS (ETH-), nm = not measured.

Tree-ring date		Site	Tree number and ring	Laboratory code	Radiocarbon age (BP)	$\delta^{13}\text{C}$ (‰)	Statistical consistency (Ward and Wilson 1978)
(AD)	(cal BP)						
46	1904	Balloo, Co Down	Q837, ring 4	ETH-122582	1927 ± 16	-27.2	
51	1899	Balloo, Co Down	Q837, ring 9	GrM-29618	1967 ± 20	-24.24 ± 0.15	T' = 0.6, T'(5%) = 3.8, ν = 1
				ETH-122583	1947 ± 16	-26.4	
56	1894	Balloo, Co Down	Q815, ring 3	GrM-29626	1958 ± 18	-23.68 ± 0.15	T' = 2.8, T'(5%) = 3.8, ν = 1
				ETH-122584	1998 ± 16	-24.0	
61	1889	Balloo, Co Down	Q815, ring 8	ETH-122585	1979 ± 16	-24.8	
66	1884	Balloo, Co Down	Q815, ring 13	ETH-122586	1970 ± 16	-25.1	
71	1879	Balloo, Co Down	Q815, ring 18	ETH-122587	1927 ± 16	-23.7	
76	1874	Balloo, Co Down	Q815, ring 23	GrM-29617	1936 ± 18	-22.41 ± 0.15	T' = 0.2, T'(5%) = 3.8, ν = 1
				ETH-122588	1926 ± 16	-22.8	
81	1869	Balloo, Co Down	Q815, ring 28	GrM-29622	1935 ± 18	-23.49 ± 0.15	T' = 0.2, T'(5%) = 3.8, ν = 1
				ETH-122589	1925 ± 16	-23.9	
86	1864	Balloo, Co Down	Q815, ring 33	ETH-122590	1917 ± 16	-25.6	
91	1859	Balloo, Co Down	Q815, ring 38	GrM-29616	1943 ± 18	-23.96 ± 0.15	T' = 0.1, T'(5%) = 3.8, ν = 1
				ETH-122591	1934 ± 16	-23.8	
96	1854	Balloo, Co Down	Q815, ring 43	GrM-29621	1966 ± 18	nm	T' = 1.7, T'(5%) = 3.8, ν = 1
				ETH-122592	1935 ± 16	-24.6	
101	1849	Balloo, Co Down	Q815, ring 48	ETH-122593	1866 ± 16	-26.6	
106	1844	Balloo, Co Down	Q1081, ring 51	ETH-122594	1910 ± 16	-26.5	
111	1839	Balloo, Co Down	Q1081, ring 56	ETH-122595	1913 ± 16	-25.3	
116	1834	Balloo, Co Down	Q821, ring 3	ETH-121928	1910 ± 15	-25.9	
121	1829	Balloo, Co Down	Q821, ring 8	GrM-29206	1922 ± 20	-23.71 ± 0.15	
126	1824	Balloo, Co Down	Q821, ring 13	GrM-29207	1872 ± 20	-24.83 ± 0.15	T' = 0.0, T'(5%) = 3.8, ν = 1
				ETH-121929	1870 ± 15	-25.7	
131	1819	Balloo, Co Down	Q821, ring 18	GrM-29208	1885 ± 20	-23.36 ± 0.15	T' = 0.6, T'(5%) = 3.8, ν = 1
				ETH-121930	1865 ± 15	-24.4	
136	1814	Balloo, Co Down	Q821, ring 23	GrM-29209	1877 ± 20	-25.03 ± 0.15	

(Continued)

Appendix 1. (Continued)

Tree-ring date		Site	Tree number and ring	Laboratory code	Radiocarbon age (BP)	$\delta^{13}\text{C}$ (‰)	Statistical consistency (Ward and Wilson 1978)
141	1809	Balloo, Co Down	Q821, ring 28	GrM-29211	1861 ± 20	-26.26 ± 0.15	
146	1804	Balloo, Co Down	Q821, ring 33	GrM-29212	1870 ± 20	-25.60 ± 0.15	T' = 0.2, T'(5%) = 3.8, ν = 1
				ETH-121931	1860 ± 15	-27.0	
151	1799	Balloo, Co Down	Q821, ring 38	GrM-29213	1867 ± 20	-25.95 ± 0.15	
156	1794	Balloo, Co Down	Q821, ring 43	GrM-29214	1856 ± 20	-24.55 ± 0.15	T' = 0.1, T'(5%) = 3.8, ν = 1
				ETH-121932	1865 ± 15	-26.4	
161	1789	Balloo, Co Down	Q821, ring 48	GrM-29216	1870 ± 20	-26.13 ± 0.15	T' = 2.0, T'(5%) = 3.8, ν = 1
				ETH-121933	1835 ± 15	-24.4	
166	1784	Balloo, Co Down	Q821, ring 53	GrM-29219	1863 ± 21	-23.96 ± 0.15	
171	1779	Balloo, Co Down	Q821, ring 58	GrM-29220	1886 ± 20	-25.24 ± 0.15	
176	1774	Balloo, Co Down	Q821, ring 63	GrM-29221	1856 ± 20	-24.60 ± 0.15	T' = 0.1, T'(5%) = 3.8, ν = 1
				GrM-29225	1866 ± 21	-24.55 ± 0.15	
181	1769	Balloo, Co Down	Q821, ring 68	GrM-29222	1877 ± 20	-25.34 ± 0.15	
186	1764	Balloo, Co Down	Q821, ring 73	GrM-29223	1871 ± 21	-25.48 ± 0.15	T' = 0.2, T'(5%) = 3.8, ν = 1
				ETH-121934	1860 ± 15	-26.8	
191	1759	Balloo, Co Down	Q821, ring 78	GrM-29224	1884 ± 21	-25.77 ± 0.15	
198	1752	Balloo, Co Down	Q1081, ring 143	ETH-122596	1810 ± 16	-28.6	
203	1747	Balloo, Co Down	Q1081, ring 148	ETH-122597	1826 ± 16	-28.6	
208	1742	Balloo, Co Down	Q1081, ring 153	ETH-122598	1801 ± 16	-27.8	
211	1739	Balinderry, Co Antrim	Q9888, ring 105	ETH-127796	1826 ± 15	-25.8	
216	1734	Allistragh, Co Armagh	Q451, ring 3	ETH-127794	1841 ± 15	-23.0	
221	1729	Allistragh, Co Armagh	Q451, ring 8	ETH-127795	1832 ± 14	-23.3	
226	1724	Balinderry, Co Antrim	Q9885, ring 52	ETH-122599	1815 ± 16	-26.9	
231	1719	Balinderry, Co Antrim	Q9885, ring 57	GrM-29624	1813 ± 18	-24.99 ± 0.15	T' = 0.8, T'(5%) = 3.8, ν = 1
				ETH-122600	1834 ± 16	-24.9	
236	1714	Balinderry, Co Antrim	Q9885, ring 62	GrM-29623	1859 ± 20	-24.86 ± 0.15	T' = 1.9, T'(5%) = 3.8, ν = 1

				ETH-122601	1824 ± 16	-25.8	
241	1709	Balinderry, Co Antrim	Q9885, ring 67	ETH-122602	1764 ± 16	-25.3	
246	1704	Balinderry, Co Antrim	Q9885, ring 72	ETH-122603	1794 ± 16	-24.4	
251	1699	Balinderry, Co Antrim	Q9885, ring 77	ETH-122604	1776 ± 16	-25.5	
256	1694	Balinderry, Co Antrim	Q9885, ring 82	ETH-122605	1732 ± 16	-25.5	
261	1689	Balinderry, Co Antrim	Q9886, ring 148	GrM-30886	1736 ± 17	nm	
266	1684	Balinderry, Co Antrim	Q9886, ring 153	GrM-30888	1720 ± 17	nm	
271	1679	Balinderry, Co Antrim	Q9886, ring 158	GrM-30889	1696 ± 17	nm	
276	1674	Balinderry, Co Antrim	Q9886, ring 163	GrM-30891	1721 ± 17	nm	
281	1669	Balinderry, Co Antrim	Q9886, ring 168	GrM-31031	1717 ± 25	-24.56 ± 0.15	
286	1664	Balinderry, Co Antrim	Q9881, ring 176	GrM-30883	1743 ± 18	nm	T' = 0.0, T'(5%) = 3.8, ν = 1
				ETH-127797	1740 ± 15	-25.8	

Appendix 2. Highest Posterior Density intervals for the ring formed in AD 286 from wiggle-matching measurements from seven rings spanning 43 successive 29-, 31-, or 33-year blocks between AD 46–76 and AD 256–286 ($A_{\text{comb}} > A_n$: 26.7, n : 7 for all); intervals which do not include the true date of AD 286 are given in bold; * indicates that the IntCal20 ΔR model has poor overall agreement ($A_{\text{model}} < 60$); all ranges have been rounded outwards to the nearest year

Dated rings (AD)	Highest Posterior Density Interval (cal AD) IntCal20 (ΔR)			Highest Posterior Density Interval (cal AD) IntCal20			Highest Posterior Density Interval (cal AD) IntCal13		
	68%	95%	99%	68%	95%	99%	68%	95%	99%
46–76	276–285 (25%)	271–291 (38%)	265–312 (47%)	279–284 (10%)	275–308 (59%)	271–312 (61%)	270–278	267–292	265–292
	328–337 (43%)	297–308 (6%)	321–344(52%)	297–306 (25%)	326–337 (36%)	322–340 (38%)			
51–81	276–289 (39%)	295–304 (27%)		287–303	277–306	272–310 (97%)	270–279	267–285	264–290
	330–332 (2%)	326–337 (12%)	240–256 (1%)			324–335 (2%)			
			272–307 (83%)						
56–86	278–297	273–304 (84%)	238–252 (1%)	284–297	279–304	274–309 (97%)	272–280	268–285	265–289
		325–336 (11%)	268–309 (86%)			323–333 (2%)			
			322–342 (13%)						
61–91	278–283 (12%)	270–307	264–312 (96%)	287–300	281–305	274–311	270–278	266–282	263–286
	285–300 (56%)		314–341 (3%)						
66–96	289–300	280–309	263–317	289–301	284–306	277–314	267–275	264–278	259–283
71–101	304–314	272–277 (1%)	266–323	306–314	298–317	287–321	269–277	266–280	261–289
		292–317 (94%)							
76–106	270–277 (19%)	267–280 (27%)	262–340	304–315	293–318	270–282 (2%)	265–274	262–278	258–283
	300–313 (49%)	291–318 (68%)				288–321 (97%)			
81–111*	267–277 (46%)	265–280 (50%)	260–356	299–315	270–277 (7%)	266–282 (9%)	262–273	259–278	254–284
	295–303 (17%)	290–321 (45%)			293–318 (88%)	286–321 (90%)			
	312–315 (5%)								
86–116*	266–276 (37%)	260–281 (44%)	255–367	294–298 (6%)	268–276 (6%)	263–283 (9%)	259–272	255–277	250–284
	293–297 (7%)	288–324 (51%)		300–301 (2%)	291–318 (89%)	285–321 (90%)			
	310–318 (24%)			305–316 (60%)					
91–121*	267–275 (34%)	256–280 (49%)	250–327 (98%)	268–276 (13%)	264–279 (28%)	258–320	257–271	251–277	246–283
	310–318 (34%)	303–323 (46%)	331–361 (1%)	303–316 (49%)	292–317 (67%)				
96–126*	291–296 (2%)	270–277 (2%)	265–379	300–301 (1%)	289–321	284–371	254–273	249–282 (89%)	246–296
	305–322 (56%)	284–353 (86%)		303–316 (67%)				286–293 (6%)	
	333–345 (9%)	359–374 (7%)							
	368–370 (1%)								
101–131	317–332 (32%)	312–349 (50%)	276–297 (1%)	314–334 (58%)	310–348 (74%)	299–375	280–289	271–293	254–295
	361–373 (36%)	352–376 (45%)	305–380 (98%)	362–369 (10%)	353–372 (21%)				
106–136		280–344 (77%)	276–378	287–303 (60%)	284–341 (94%)	283–370	247–258 (48%)	243–266 (61%)	241–293
		356–375 (18%)		320–328 (8%)	359–366 (1%)		280–287 (20%)	272–291 (34%)	

	283–298 (38%) 319–334 (18%) 362–371 (12%)								
111–141	281–298 (50%) 319–324 (4%) 360–371 (14%)	279–304 (54%) 310–341 (20%) 353–375 (21%)	277–377	285–300 (52%) 316–328 (16%)	283–339 (90%) 354–366 (5%)	282–369	245–255 (33%) 276–287 (35%)	241–261 (46%) 270–291 (49%)	239–293
116–146	281–296 (42%) 314–325 (11%) 358–370 (15%)	278–301 (47%) 306–367 (24%) 345–374 (24%)	277–376	285–298 (30%) 309–331 (38%)	284–339 (83%) 343–363 (12%)	281–368	246–251 (9%) 270–286 (59%)	240–258 (26%) 266–290 (69%)	237–293
121–151	281–296 (30%) 304–331 (34%) 360–366 (4%)	280–338 (74%) 339–369 (21%)	276–373	285–295 (14%) 306–333 (47%) 343–350 (7%)	284–357	281–366	246–249 (3%) 266–286 (65%)	240–258 (21%) 261–290 (74%)	236–293
126–156	290–327 (59%) 328–330 (2%) 333–339 (7%)	282–352	279–368	308–329 (36%) 330–349 (32%)	289–354	283–363	260–283	245–291	235–325
131–161	290–319 (42%) 327–345 (26%)	279–362	273–366	306–315 (9%) 330–354 (59%)	292–358	280–362	262–281	252–294	240–347
136–166	281–319 (52%) 324–338 (16%)	273–356	267–363	301–314 (18%) 329–352 (50%)	287–355	273–358	261–279	252–308 (93%) 327–339 (2%)	246–347
141–171	282–319	266–332	264–352	291–324	275–346	268–351	257–284	230–236 (1%) 253–335 (94%)	223–341
146–176	267–271 (3%) 283–319 (65%)	263–325	259–349	291–323	268–329 (91%) 334–341 (4%)	264–346	256–279	233–244 (3%) 252–329 (92%)	220–335
151–181	260–270 (15%) 287–314 (53%)	258–318	253–345	287–317	261–322	257–399	219–231 (12%) 254–279 (56%)	215–244 (21%) 251–295 (65%) 299–323 (9%)	213–329
156–186	258–270 (21%) 284–285 (1%) 287–311 (46%)	256–314	251–325	284–315	258–318	254–331	219–237 (23%) 254–277 (45%)	214–244 (30%) 251–291 (53%) 293–318 (12%)	211–324
161–191	256–269 (23%) 280–303 (45%)	252–308	246–321	259–262 (4%) 278–309 (64%)	255–312	250–322	208–236 (66%) 257–261 (2%)	204–248 (75%) 250–280 (15%) 296–313 (5%)	203–317
166–198	294–315 (62%) 323–329 (6%)	247–276 (14%) 288–333 (81%)	241–335	300–314	266–277 (1%) 290–328 (94%)	248–330	224–240	217–258	214–287 (97%) 292–318 (2%)
171–203	296–313 (62%) 321–326 (6%)	290–332	240–333	301–314	297–322	288–329	225–239	217–251	216–283 (98%) 293–316 (1%)
176–208	297–311 (50%) 320–327 (18%)	295–329	289–334	305–319	299–324	294–328	222–241 (47%) 299–312 (21%)	220–273 (68%) 295–316 (27%)	217–319
181–211	298–312	294–324	290–329	304–314	299–319	294–323	221–237 (61%) 300–307 (7%)		217–282 (81%) 285–315 (18%)

(Continued)

Appendix 2. (Continued)

Dated rings (AD)	Highest Posterior Density Interval (cal AD) IntCal20 (ΔR)			Highest Posterior Density Interval (cal AD) IntCal20			Highest Posterior Density Interval (cal AD) IntCal13		
	68%	95%	99%	68%	95%	99%	68%	95%	99%
186–216	297–307	292–313	288–323	301–309	297–313	293–317	221–237 (46%) 256–270 (18%) 297–302 (4%)	219–243 (68%) 250–273 (10%) 293–312 (17%) 219–277 (83%) 290–306 (12%)	218–309
191–221	296–304	292–309	287–315	298–306	295–309	292–313	220–236 (30%) 249–274 (38%)	218–281 (88%) 286–300 (7%)	217–304
198–226	295–303	292–308	287–314	298–305	295–308	292–312	230–242 (14%) 246–280 (54%)	223–296	219–302
203–231	291–300	286–304	281–309	294–300	290–303	287–306	229–254 (33%) 255–278 (35%)	217–289	213–296
206–236	284–295	278–300	270–304	288–295	284–298	281–301	229–271	213–279	209–288
211–241	282–293	279–299	273–304	286–293	283–297	280–300	268–288	216–242 (11%) 257–291 (84%)	206–293
216–246	280–291	276–297	270–301	284–291	281–294	277–297	272–285	225–230 (1%) 258–291 (94%)	200–243 (4%) 252–293 (95%)
221–251	280–290	276–295	270–299	283–290	280–293	277–296	275–285	268–289	257–293
226–256	282–292	278–296	273–300	285–291	282–293	279–296	279–288	274–291	270–293
231–261	283–293	279–296	274–300	285–290	282–293	279–295	280–288	276–291	271–293
236–266	283–293	278–297	274–299 (97%) 350–370 (2%)	284–290	281–294	279–296 (97%) 349–363 (2%)	282–289	278–292	273–293
241–271	282–291 (32%) 354–366 (36%)	278–294 (39%) 345–375 (56%)	276–297 (40%) 339–384 (59%)	285–291 (28%) 356–365 (40%)	282–294 (38%) 352–370 (57%)	280–296 (39%) 347–375 (60%)	285–291 (24%) 348–358 (44%)	281–294 (37%) 345–361 (58%)	277–297 (39%) 340–366 (60%)
246–276	279–291 (59%) 356–361 (9%)	277–293 (65%) 348–373 (30%)	274–295 (66%) 341–383 (33%)	282–291 (63%) 359–361 (5%)	280–292 (70%) 354–368 (25%)	278–294 (71%) 348–374 (28%)	281–290 (41%) 349–356 (27%)	278–293 (52%) 349–356 (43%)	275–296 (54%) 340–365 (45%)
251–281	281–289 (22%) 354–373 (46%)	277–291 (28%) 345–386 (67%)	274–294 (28%) 340–409 (71%)	283–288 (19%) 358–370 (49%)	280–291 (30%) 353–375 (65%)	278–294 (31%) 348–385 (68%)	283–289 (15%) 347–359 (53%)	279–293 (28%) 343–363 (67%)	275–299 (30%) 337–370 (69%)
256–286	280–290 (32%) 360–364 (5%) 366–382 (31%)	278–291 (34%) 356–404 (61%)	276–294 (35%) 342–407 (64%)	281–289 (32%) 358–372 (36%)	279–291 (39%) 355–380 (56%)	276–295 (40%) 347–393 (59%)	280–294	277–302 (81%) 344–363 (14%)	274–312 (82%) 336–380 (17%)